(12)

THERMOMECHANICAL CONTACT PHENOMENA AND WEAR OF SLIDING COMPONENTS

by

Francis E. Kennedy, Jr.
Associate Professor of Engineering

and

Syed Z. Hussaini and Beda M.M. Espinoza
Graduate Research Assistants

Annual Report

submitted to

Office of Naval Research
Contract No. N00014-81-K-0090
Period Covered: January 1, 1986 to December 31, 1986

March 27, 1987

THAYER
SCHOOL OF
ENGINEERING
TH COLLEGE

Unclassified
SECURITY CLASSIFICATION OF THIS PAGE

AD-A180 487

REPORT DOCUMENTATION PAGE

1a. REPORT SECURITY CLASSIFICATION Unclassified	1b RESTRICTIVE MARKINGS
2a SECURITY CLASSIFICATION AUTHORITY	3 DISTRIBUTION / AVAILABILITY OF REPORT Approved for public release; distribution unlimited
2b DECLASSIFICATION / DOWNGRADING SCHEDULE	
4 PERFORMING ORGANIZATION REPORT NUMBER(S) Annual Report 1986	5 MONITORING ORGANIZATION REPORT NUMBER(S)
6a NAME OF PERFORMING ORGANIZATION Dartmouth College 6b OFFICE SYMBOL (If applicable)	7a NAME OF MONITORING ORGANIZATION Office of Naval Research
6c. ADDRESS (City, State, and ZIP Code) Thayer School of Engineering Hanover, NH 03755	7b ADDRESS (City, State, and ZIP Code) Engineering Science Directorate Arlington, Virginia 22217
8a. NAME OF FUNDING / SPONSORING ORGANIZATION Office of Naval Research 8b OFFICE SYMBOL (If applicable)	9 PROCUREMENT INSTRUMENT IDENTIFICATION NUMBER N00014-81-K-0090
8c. ADDRESS (City, State, and ZIP Code) Engineering Science Directorate Arlington, Virginia 22217	10 SOURCE OF FUNDING NUMBERS PROGRAM ELEMENT NO: 61153N 24 PROJECT NO: NR 091-044 TASK NO: RR024-03-03 RMS2403-032 WORK UNIT ACCESSION NO:

11 TITLE (Include Security Classification)
Thermomechanical Contact Phenomena and Wear of Sliding Components

12 PERSONAL AUTHOR(S)
Francis E. Kennedy, Jr. Syed Z. Hussaini, Beda M.M. Espinoza

13a TYPE OF REPORT	13b TIME COVERED	14 DATE OF REPORT (Year, Month, Day)	15. PAGE COUNT
Annual Report	FROM 86/1/1 TO 86/12/31	1987 March 27	

16 SUPPLEMENTARY NOTATION

17 COSATI CODES			18 SUBJECT TERMS (Continue on reverse if necessary and identify by block number)
FIELD	GROUP	SUB-GROUP	
11	01		Mechanical Seals, Face Seals, Wear, Friction, Ceramics, Thermal Stress

Silicon carbide

19 ABSTRACT (Continue on reverse if necessary and identify by block number)

The objectives of this work have been to gain a better understanding of the wear of solid ceramic and ceramic-coated metallic seal rings in contact with carbon graphite and to determine the solid/solid contact conditions responsible for that wear. Ring-on-ring sliding tests were run under dry conditions (no sealed fluid) with carbon graphite seal rings sliding against two types of hard seal face materials, monolithic silicon carbide and metallic materials coated with either tungsten carbide or titanium nitride. The total wear of the hard ring materials was very low in all cases, with reaction-sintered SiC and TiN-coated rings having the lowest total wear. There was less wear of the carbon graphite rings when they were run against coated rings than when in contact with SiC. In the analytical phase of this work, the temperature and stress distributions in the sliding contact region were determined using finite element methods. It was shown that frictional heating is the dominant contributor to high localized stresses in the contact region, that plastic deformation can occur in the region, and that thermal deformations and stresses can be a major reason for coating failure. The influence of coating and substrate properties, as well as coating thickness, on the results and on potential failure mechanisms was studied.

Titanium Nitride

20. DISTRIBUTION / AVAILABILITY OF ABSTRACT	21. ABSTRACT SECURITY CLASSIFICATION
☒ UNCLASSIFIED/UNLIMITED ☐ SAME AS RPT ☐ DTIC USERS	Unclassified
22a NAME OF RESPONSIBLE INDIVIDUAL P. J. Blau	22b TELEPHONE (Include Area Code) (202) 696-4401
	22c. OFFICE SYMBOL ONR Code 431

DD FORM 1473, 84 MAR 83 APR edition may be used until exhausted. All other editions are obsolete

SECURITY CLASSIFICATION OF THIS PAGE

THERMOMECHANICAL CONTACT PHENOMENA AND WEAR OF SLIDING COMPONENTS

Annual Report 1986

submitted to

Office of Naval Research

Contract No N00014-81-K-0090
Period Covered: January 1, 1986 to December 31, 1986

by

Francis E. Kennedy, Jr.
Associate Professor of Engineering

and

Syed Z. Hussaini and Beda M.M. Espinoza
Graduate Research Assistants

Thayer School of Engineering
Dartmouth College
Hanover, New Hampshire 03755

March 1987

FOREWORD

Work at the Thayer School of Engineering at Dartmouth College on this research project has been sponsored by Office of Naval Research Contract Number N00014-81-K-0090. Dr. Peter J. Blau has been the ONR Scientific Officer for the project during the past year.

The authors gratefully acknowledge the assistance of V.A. Surprenant and the personnel of the Dartmouth Electron Microscope Facility in metallographic work. Several individuals and companies contributed materials and advice during the experimental work: J.A. Sue of Union Carbide Corp., J.E. Garnier of Sohio Engineered Materials Co., J.P. Netzel of Crane Packing Co., H.F. Greiner of EG&G Sealol, and A. Massaro of Pure Carbon Co.

TABLE OF CONTENTS

LIST OF FIGURES

LIST OF TABLES

1.0 INTRODUCTION

Whenever flat, conforming rings are placed together and sliding commences, there is solid-solid contact between the rings in small, discrete spots which constitute the real area of contact. This solid-solid contact occurs whether the contacting rings are dry, as in annular disk brakes, or "lubricated", as in mechanical face seals. The thin layer of sealed fluid which is assumed to be present between the seal faces in the latter application does not prevent contact between the flat seal rings [1,2]. The solid-solid contact is responsible for much of the friction which occurs between the sliding rings and is also the origin of the mechanical consequences of friction, i.e., frictional heating, near-surface plastic deformation, and wear of the contacting ring surfaces. The resulting wear can be the cause of early failure of the sliding components. To overcome the wear problem, a number of hard, wear-resistant ceramic materials have been developed for use in mechanical face seals and other sliding conforming contacts. The ceramics and ceramic coatings have met with varying degrees of success in these applications. In addition to wear, other failure modes, particularly thermocracking or heat checking, can be caused by the thermal and mechanical sliding contact phenomena, and some such failures have been observed with ceramic or ceramic-coated rings.

The objective of this work has been to gain a better understanding of the wear and thermocracking of solid ceramic and ceramic-coated rings in dry sliding contact. Of particular interest were rings of the type being considered for use in mechanical face seals, where they would likely be in contact with seal rings made from carbon graphite. An experimental program of sliding tests was conducted with ceramic or ceramic-coated rings in contact with carbon graphite rings. In order to better understand the tribological failure of the sliding rings it was deemed desirable to characterize the solid-solid contact conditions at the sliding interface and to study the temperatures, stresses, and deformations that arise near those contacts as a result of friction. Finite element thermal and thermomechanical anslyses were performed for that purpose.

2. EXPERIMENTAL STUDY

2.1 INTRODUCTION TO THE EXPERIMENTAL STUDY

The approach used in this investigation of solid ceramics and ceramic coatings was one used in an earlier study of the wear of metallic seal rings [3]. Because wear occurs only in the regions of actual solid/solid contact, it is desirable to know how large those contact patches are, how they are distributed on the seal interface, what are the conditions within the contact patches, and how those conditions relate to measured wear and friction. That information was obtained in this study, as in the previous one, by means of a specially-designed contact probe [1]. The probe enables acquisition of data about actual contact conditions during face seal operation. Since wear occurs only at solid contacts, and since an earlier study [3] had shown that the presence of a sealed fluid does not substantially alter the size of the solid/solid contacts, it was decided to run all tests dry, i.e., without a sealed fluid.

2.2 EXPERIMENTAL TECHNIQUES

2.2.1 Apparatus

The experiments were carried out on a converted 2-spindle drill press, with each spindle driven by a separate 2 horsepower motor. Normal load was applied through the spindles by static weights hung on the loading arm. Beneath each spindle was a specimen-holding platform mounted on a thrust bearing. Rotation of the specimen holders was limited by a torque-sensing system for friction determination.

All tests were run with a ring-on-ring specimen configuration. Test rings of various materials, with a mean diameter of approximately 5 cm. and a face width of at least 2.5 mm, were mounted in specimen holders on both the test platform and the end of the rotating spindle. The stationary ring was made of carbon graphite and had a face width of 2.5 mm and a shape typical of commercial seal rings. In some cases it had a very small (0.22 mm diameter) hole drilled in it, perpendicular to the contact surface. A fine (0.18 mm diameter) wire was inserted in the hole and bonded in place with an electrically insulating epoxy adhesive, prior to having its surface lapped and polished. The wire then formed part of the ring surface, but it was electrically insulated from the rest of the ring. Operation of the contact probe is described elsewhere [1].

Weight measurements of the test rings before and after tests enabled determination of total wear of

each ring. Information about wear at specific locations (within the contact patches) and the inter-relationship between wear and surface profile was gained with the aid of a computer-assisted stylus profilometry system [3]. Some linear profiles were taken in the radial direction, while other profiles were circumferential, with a high accuracy, motor-driven, air bearing rotary table being used to rotate the ring-shaped specimens beneath the profilometer's stationary stylus. A real-time data acquisition system was used to acquire and digitize the surface profile data and to pass the data to a digital computer for analysis and plotting.

2.2.2 Materials

Two monolithic ceramics were studied, both of the silicon carbide family. The first was a commercial seal ring material, reaction-sintered silicon carbide. Microscopic examination revealed that the material had a mean SiC grain size of 10 - 15 μm and contained about 15 - 20% free silicon. The second silicon carbide material was a sintered particulate composite of silicon carbide and titanium di-boride. The material contained about 20 weight percent TiB_2, with both SiC and TiB_2 grains having a grain size in the range 2 to 5 μm. Although this new material has not yet been used in face seal applications, it was chosen for this study because it has higher electrical conductivity than sintered or reaction-bonded grades of silicon carbide. The improved conductivity enabled use of our contact probe to study contact conditions at the carbon graphite / silicon carbide interface. The SiC + TiB_2 material also has greater fracture toughness than many other grades of silicon carbide.

The ceramic coatings that were investigated were tungsten carbide and titanium nitride. Two different tungsten carbide coatings were studied, both of which had a cobalt binder and were applied by high velocity thermal spray processes which produce dense, high quality coatings. The first had 12% cobalt and was applied to a mild steel substrate while the second had 14% cobalt and was on a beryllium copper substrate. All tungsten carbide coatings were approximately 0.25 mm thick after spraying and slightly thinner after lapping.

The titanium nitride coatings were applied by a physical vapor deposition (PVD) process to previously-lapped beryllium copper substrates. Coating was done by means of vacuum arc deposition at

a coating temperature of 485 °C. The TiN coatings were between 5 and 7 μm thick.

All of the wear-resistant rings were tested against seal rings made from the same resin- impregnated grade of carbon graphite. Although it is usually wise to choose a grade of carbon graphite which is most compatible with the mating ring material, it was decided to use a single grade in these tests to eliminate a test variable.

2.2 3 Procedures

Before each test of a silicon carbide or tungsten carbide-coated ring, the ring surface was hand lapped using a diamond lapping/polishing compound (1 μm grit). The titanium nitride surfaces were not re-lapped after coating because of their thinness. All rings, including the carbon graphite rings, had their surface topography characterized before each test using the computer-assisted profilometry system. The rings were washed in a non-abrasive cleaner and then ultrasonically cleaned in ethanol and dried before being weighed on an analytical balance.

During a test the carbon graphite ring was mounted in the stationary specimen, while the wear-resistant ring was mounted on the rotating holder. Most tests were run at a speed of 188.5 s^{-1} (1800 rpm), giving a sliding velocity of 4.7 m s^{-1}, although some tests of WC- or TiN-coated rings were also run at a sliding velocity of 3.1 m s^{-1}. A normal force of 100 N was applied to the rings in all tests, giving a nominal pressure of 0.25 MPa between the contact faces. The total sliding distance for most tests was 200 km, for a test duration of approximately 12 hours. For each material combination there were at least six tests of 12 hour duration, along with one test lasting 30 hours (500 km) and several of shorter duration (17 km). The friction force was monitored continuously during each test. The contact probe was used occasionally during the tests of all materials except reaction-sintered SiC to monitor the size and location of the regions of solid/solid contact between the rings.

At the conclusion of a test the seal was disassembled and each ring was ultrasonically cleaned and dried. The rings were each reweighed on the analytical balance and the surface topography of each was again characterized. The ring surfaces were examined using an optical microscope and, in some cases, a scanning electron microscope.

2.3 EXPERIMENTAL RESULTS AND DISCUSSION

2.3.1 Reaction-Sintered Silicon Carbide

The tests of reaction-sintered silicon carbide rings were characterized by periods of smooth sliding punctuated every 10 to 15 minutes by short bursts of much higher friction accompanied by a grinding sound and some vibration. The friction coefficient was generally between 0.10 and 0.11, but increased to 0.25 to 0.4 during the bursts, which generally lasted 5 or 10 seconds. During one such disturbance the test was stopped intentionally to observe the sliding surfaces. Large patches of carbon wear debris were clearly observed on the SiC surface, although no such debris patches were observed when the test was stopped during periods of smoother, lower friction. Wear of the silicon carbide rings was very low, with a mean wear rate of 0.0094 mg/km of sliding. Since the contact area was about 400 mm^2, the mean linear wear rate was only 0.008 μm/km. The wear was also unsteady though, and the standard deviation of the wear rate was approximately equal to the mean value. In some tests, in fact, the wear rate was so small that it was nearly undetectable with our mass measurement techniques. The carbon graphite, on the other hand, exhibited rather high wear, higher than with any of the other hard faces tested here. The mean carbon graphite wear rate was 2.05 mg/km, which translates to a linear wear rate of 2.8 μm/km.

Observation of the silicon carbide surfaces after the sliding tests revealed the presence of some thin wear grooves or scratches on the SiC surface. Two examples of such scratches are shown in Figure 1. Close examination of the scratches showed that each had been caused by a silicon carbide particle which had pulled out and scratched the surface. Carbon wear debris had then collected in the scratches, as can be seen in Fig. 1. Further evidence of the presence of scratches was obtained by characterizing the topography of the SiC surface. Radial surface profiles of the surface before and after a 12 hour test showed the height distributions plotted in Figure 2. The post-test surface profile was taken across one of the scratches and showed many samples within the valleys. There was generally only a negligible increase in maximum peak-to-valley height, but the roughness average (Ra) increased by 10% to 20%. The pulled-out SiC particles evidently had remained trapped between the two rings for a period of time and appeared to be responsible for the significant wear of the carbon graphite rings. The surface roughness (Ra) of the carbon rings was found to increase by about 25% during the tests against the

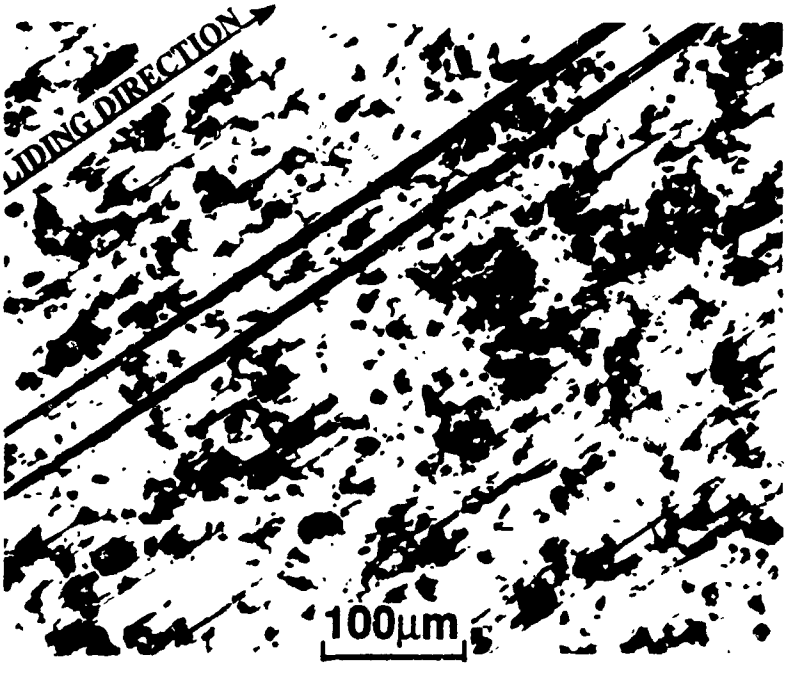

Figure 1 Optical micrograph of worn SiC (reaction-sintered) surface.

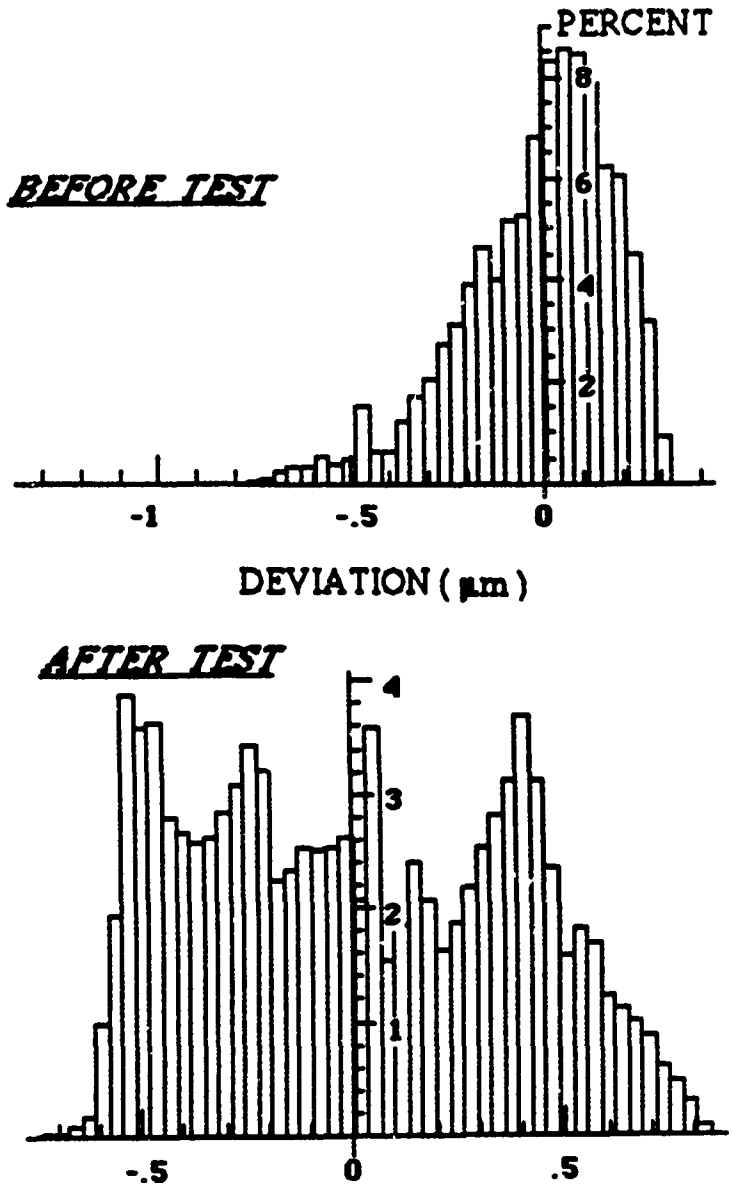

Figure 2 Distribution of heights (deviation from centerline) for SiC surface before and after sliding test.

silicon carbide rings and this is consistent with the idea that pulled-out SiC grains were responsible for much of the wear of the carbon graphite. It might be noted that some pullout has been noted by other researchers [10] during sliding tests of silicon carbide under loads even lower than the 100 N used in our tests.

2.3.2 Silicon Carbide plus Titanium Di-Boride

Although this sintered composite material was different in composition from the reaction-sintered silicon carbide, its sliding contact behavior was quite similar. As with the SiC material, the SiC + TiB_2 rings showed periods of smooth contact with a coefficient of friction about 0.10, punctuated every 10 or 15 minutes by a short (10 seconds or so) burst of higher friction. Friction during the bursts rose to about 0.25 and there was some accompanying noise and vibration, but not as much as in the tests of SiC.

Because SiC + TiB_2 has much better electrical conductivity than SiC, the contact probe could be used in the tests of the SiC + TiB_2 material. During operation of the probe a 5 volt DC signal was produced whenever a point on the rotating hard ring was in contact with the probe wire location on the stationary carbon graphite ring, but there was no signal (zero volts) if there was no contact. By monitoring the probe output signal for each complete rotation of the ring one could determine which portions of the rotating ring surface were in solid/ solid contact with the carbon ring surface, or at least with that point on the carbon surface where the probe wire was located. A typical contact probe output for a SiC + TiB_2 ring is shown in Figure 3. It can be seen that many individual asperity contacts were occurring, but the contacts were grouped together within one large patch which covered nearly 30% of the ring circumference. The patch location remained approximately fixed relative to the SiC + TiB_2 ring over many revolutions. As the friction burst was about to occur, however, the patch size seemed to grow until it covered nearly 100% of the ring circumference. By carefully observing the output from the contact probe, it was determined that the supposed 100% contact between SiC + TiB_2 ring and carbon graphite ring was actually large-scale contact between each ring and an intermediate conductive third body, causing leakage of the probe signal across the gap between the rings. Presumably the conductive third body was the carbon graphite wear debris noted during the SiC tests.

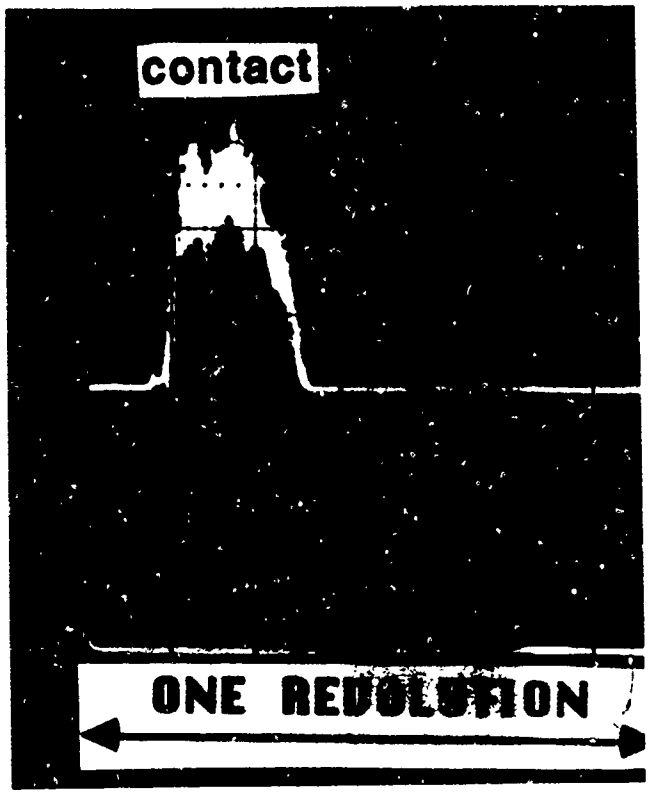

Figure 3 Typical contact probe output for SiC + TiB_2

TABLE 1

RESULTS OF SLIDING WEAR TESTS

SLIDING VELOCITY: 4.71 m/s SLIDING DISTANCE per TEST: 200 km
APPLIED NORMAL LOAD: 100 N (0.25 MPa)

COUNTERFACE	CARBON GRAPHITE		
MATERIAL	WEAR RATE mg/km	WEAR RATE mg/km	FRICTION COEFFICIENT
SiC + Si (15%)	0.0094 (σ=0.0098)	2.05 (σ=0.87)	0.10-0.11
SiC + TiB_2	0.021 (σ=0.04)	0.43 (σ=0.12)	0.10-0.12
WC + Co (12%) (on steel)	0.037 (σ=0.0095)	0.19 (σ=0.086)	0.09 - 0.10
WC + Co (14%) (on BeCu)	0.029 (σ=0.017)	0.54 (σ=0.41)	0.09 - 0.10
TiN (on BeCu)	0.0055 * (σ=0.0067)	0.41 (σ=0.20)	0.10 - 0.20

* values measured before coating failure

Standard deviations of wear rates are shown in parentheses.

At least six tests were run for each set of materials.

Wear data for the SiC + TiB_2 material, given in Table 1, were low, but erratic, as had been the case with SiC. There was a tendency for the SiC + TiB_2 to wear more than SiC, but there were also some tests in which the wear was too small to be measured accurately. On the other hand, the carbon graphite wear data given in Table 1 were quite consistent and showed that there was over 4 times less wear of the carbon ring when running against SiC + TiB_2 than when sliding against SiC. That result is related to the wear process for the two silicon carbide materials, which was primarily by pullout of hard ceramic grains. Whereas with the SiC material the pulled-out particles were relatively large SiC grains, with SiC + TiB_2 the pullout was of much smaller grains, which caused less abrasion damage to the carbon graphite surface. As can be seen in Figure 4, there were numerous scratches on the surface of the SiC + TiB_2 ring caused by the pulled-out particles, but it could not be determined whether SiC or TiB_2 particles were responsible for the majority of the scratches. Because of the scratches there was an increase in the surface roughness (Ra) of the SiC + TiB_2 rings.

2.3.3 Tungsten Carbide

Tests of the tungsten carbide-coated steel rings showed that contact conditions and friction were both periodic. During a period, which lasted about an hour, the friction coefficient varied from 0.09 to 0.14 and then back to 0.09. The contact probe showed that when the friction was lowest solid/solid contact occurred over a very small percentage of the contact interface. As can be seen in Figure 5a, numerous asperity-level contacts were concentrated in one patch covering about 25% of the circumference of the coated ring. As the test progressed the contact patch began to grow, as shown in Figure 5b. Soon after the condition shown in Fig. 5b the patch had apparently expanded to cover nearly 100% of the ring circumference, at which time the friction was highest. By observing the contact surfaces and the current leakage from the contact it was found that, as was the case with the silicon carbide rings, the reason for the appearance of contact over nearly the entire circumference was the presence of a conductive third body, carbon graphite wear debris, between the two ring surfaces. Soon after widespread three-body contact was observed, the friction dropped back to its lower value and the contact returned to the two-body condition shown in Figure 5a, probably owing to the loss of carbon wear debris from the contact interface.

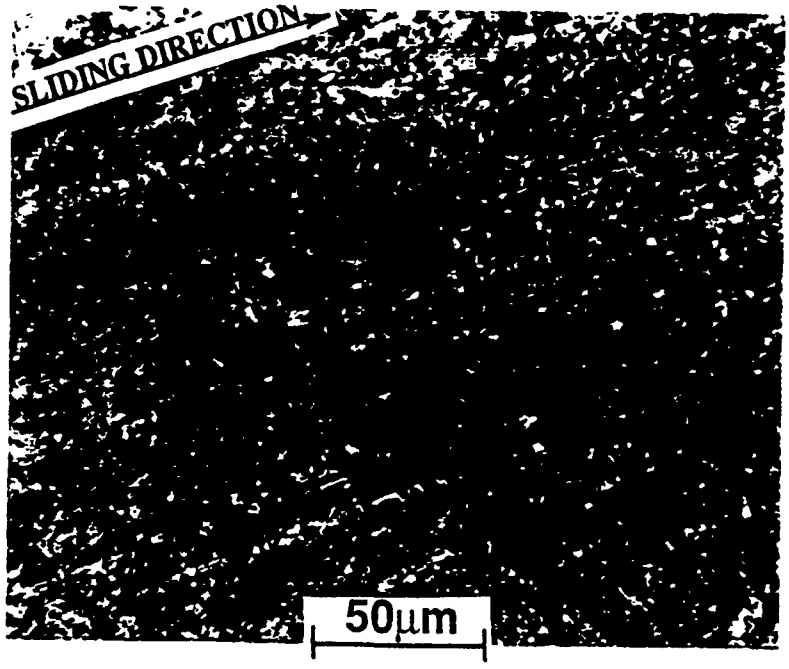

Figure 4 Optical micrograph of worn surface of SiC + TiB_2

Figure 5 Contact probe output for WC-coated steel ring sliding against carbon graphite

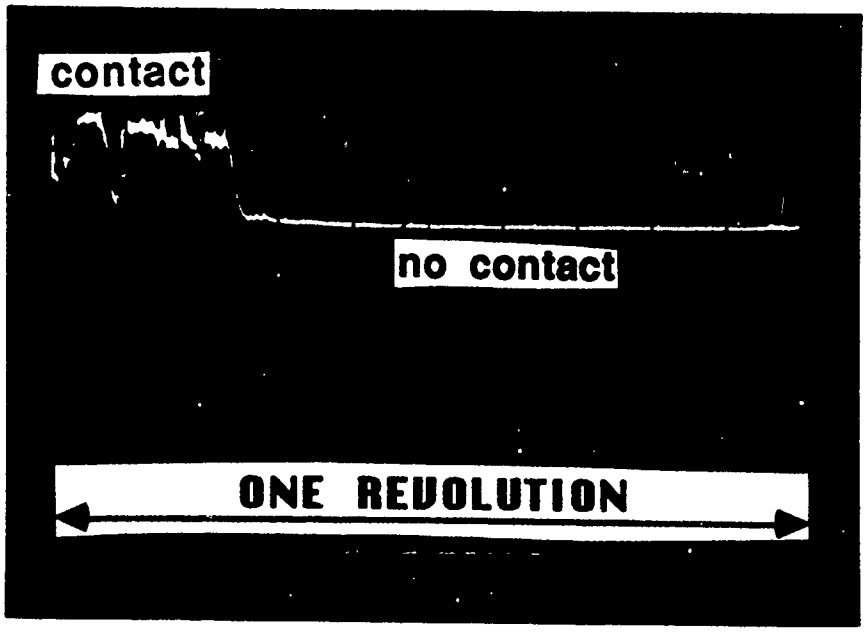

a. Contact probe output at 4:00 pm.

b. Contact probe output at 4:37 pm.

Wear of the tungsten carbide-coated rings was found to be somewhat greater than with silicon carbide, but still quite low in comparison to metallic seal ring materials tested in earlier work [3]. The average wear rate for the tungsten carbide-coated steel rings was 0.037 mg/km while that of the mating carbon graphite rings was 0.19 mg/km. Thus, as can be seen in Table 1, considerably less wear of the carbon ring occurred with tungsten carbide coatings than with either type of silicon carbide. Although most sliding tests of the WC-coated steel rings were run at a velocity of 4.7 m s^{-1}, a few tests were also conducted at 3.1 m s^{-1}. It was found that the slower tests resulted in more wear of the carbon graphite rings (0.37 mg/km) but less tungsten carbide wear (0.017 mg/km). Friction, contact conditions, and surface appearance were similar at both sliding speeds.

Microscopic examination and profilometric measurements of the tungsten carbide surfaces before and after the wear tests showed that the worn surfaces had become polished. The surface roughness (Ra) of the coating decreased in each test by between 35% and 55%. The surface profiles and the distribution of heights showed that the change in roughness could be attributed to a wearing of the peaks, with little, if any, change occurring in the valleys. A similar conclusion could be reached by examining the surfaces in an optical microscope, as in Figures 6a and 6b. Although a few small scratches are visible on the worn surface (Fig. 6b), the dominant feature of that surface is a polished appearance resulting from the wear process.

Measurement of the microhardness of the tungsten carbide coating showed that there was an insignificant difference between the coating hardness before and after a sliding test. Both hardness values were between 1100 and 1200 Vickers.

Tests were also run with a slightly different tungsten carbide coating on a substrate of beryllium copper. Contact conditions with that ring material were similar to those observed with WC on steel; i.e., generally there was contact only within several patches that covered about 20% of the ring surface but occasionally the region in which contact was occurring extended to cover the entire ring surface, at which time contact was through a third body (carbon wear debris) and friction was a bit higher. Friction coefficients were about the same as for the slightly different WC coating on a steel substrate. Wear of the WC + 14% Co coating on BeCu was very slightly less than that of the WC + 12% coating on steel. More

Figure 6 Optical micrograph of surface of WC coating on steel substrate

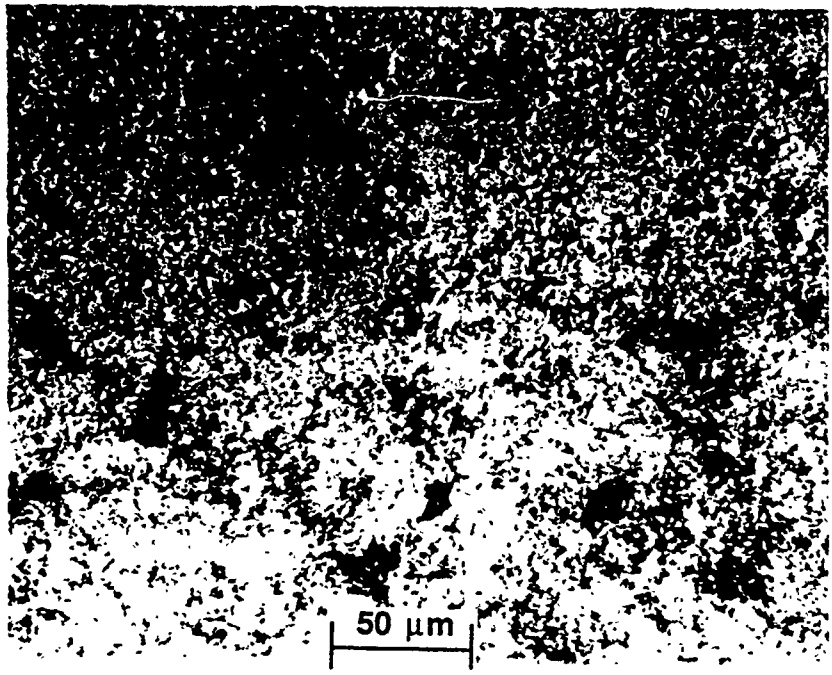

a. Before test

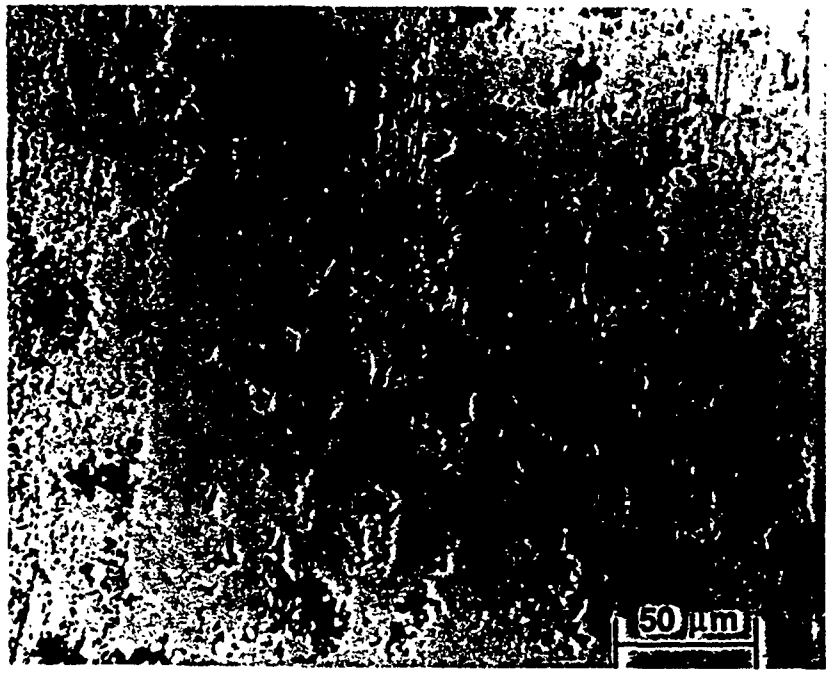

b. After test

significant was the increase, noted in Table 1, of the wear rate of the carbon graphite against the WC-on-BeCu surface. The reason for the higher carbon graphite wear against WC-on-BeCu is not clear, since both WC coatings showed a decrease in surface roughness (Ra) resulting from a polishing-type wear process, with few if any scratches indicative of the presence of hard, abrasive wear debris.

2.3.4 Titanium Nitride

The tests of titanium nitride-coated rings were quite smooth and had fewer friction transients than the other materials tested in this program. The friction coefficient was generally about 0.08-0.10 with an occasional increase to 0.15. The TiN coatings were very wear resistant and had consistently low wear rates as long as the coatings remained intact. In fact the mean wear rate, 0.0055, was of the same order of magnitude as that of silicon carbide. The wear of the carbon graphite rings in contact with TiN coatings was about the same order of magnitude as that found in tests of SiC + TiB_2 or tungsten carbide, and much less than with reaction-sintered SiC. The wear data tabulated in Table 1 for the TiN tests were those values measured before coating failure. Although the wear of the coating was very small, it was measureable and resulted in a thinner coating. For two of the TiN-coated rings tested, by the conclusion of the test program the coating had worn through to the substrate in several places. After the coating had worn through, the wear rates of both TiN-coated ring and carbon graphite rose significantly. Thus, the long term durability of such thin coatings is of concern.

In general the wear process of the TiN coatings was a polishing-type wear. The coating surface became smoother during almost all tests, although the roughness decrease was less than that noted with WC coatings. In particular, most TiN surfaces which started out with Ra < 0.15μm tended to get a bit rougher, while those originally rougher than Ra = 0.15μm became polished and ended up with a smoother surface. There was no definite pattern of roughness change for the carbon graphite surfaces in these tests.

Microscopic examination of the TiN surfaces after the tests showed that there were few grooves or scratches on the surfaces. There was some carbon transfer, as there had been with the other hard materials. Microscopic examination also revealed, in several instances, the presence of small spalled

Figure 7a Scanning electron micrograph of spalled area of TiN coating

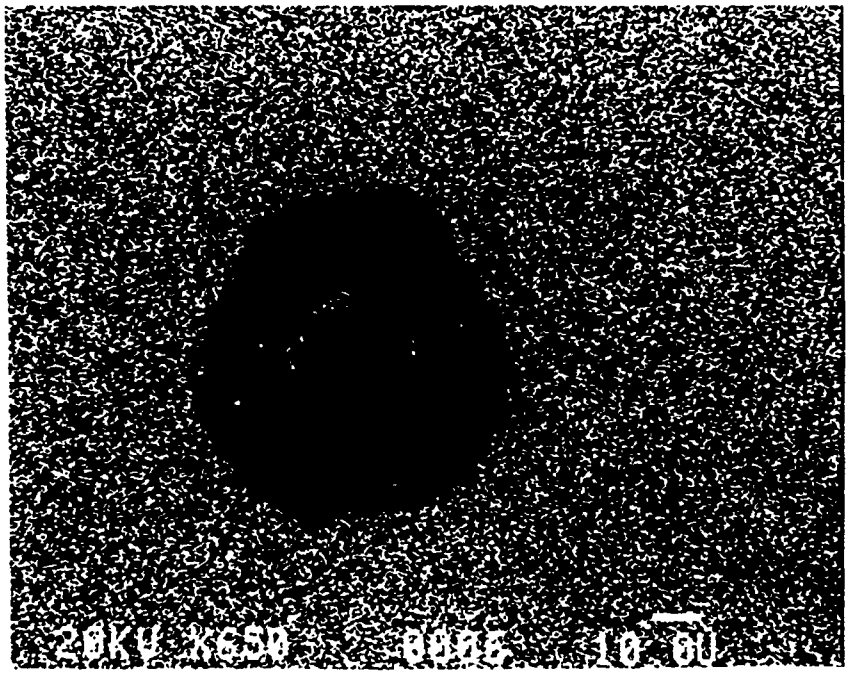

Figure 7b Energy dispersive X-ray analysis dot map showing presence of titanium in region shown in Figure 7a

regions of the coating. One such spall is shown in Figure 7, which also shows an elemental analysis of the presence of titanium in the region, obtained by energy dispersive x-ray analysis. It can be seen the nearly circular central spall, approximately 65 μm in diameter, was the result of a separation of the coating from the substrate (a typical adhesive failure [9]). Such a failure probably originated at a point where the adhesion of coating to substrate was weaker than elsewhere. There also appears to be some decohesion of the coating in a tri-lobed region around the central spall, although that was not seen at all spall locations and may have followed the initial de-adhesion of the central region. Spalls of the type seen in Figure 7 were more prevalent after some wear of the TiN coating had occurred and the coating had become thinner. It is likely that the spall event resulted in the presence of crushed TiN debris in the interfacial region and that debris could have caused some wear of the carbon graphite ring.

2.4 CONCLUSIONS FROM EXPERIMENTAL STUDY

The conclusions of this experimental program can be summarized as follows:

(1). Contact conditions at the interface between a hard, wear-resistant ring (ceramic or ceramic-coated) and a carbon graphite ring were non-uniform, with contact size varying periodically from < 10% of the ring surface, in which many small asperity-sized spots of solid/solid contact occurred, to nearly 100% of the ring surface, at which time a thin layer of carbon wear debris separated the two surfaces.

(2). Friction for all material combinations tested was low (0.10 or slightly less) except at those times when a third body layer of carbon wear debris separated the ring surfaces. At those times bursts of higher friction were noted. The friction coefficient during those bursts jumped to as high as 0.30 with silicon carbide rings.

(3). The most wear-resistant materials tested in the program were silicon carbide and TiN coatings, with wear of those materials being 3 or 4 times less than that of tungsten carbide coatings. The addition of titanium di-boride to the silicon carbide resulted in an increase in wear rate.

(4). The rings coated with tungsten carbide or titanium nitride tended to wear mainly by a process of polishing of the surface asperities, while the silicon carbide rings tended to wear by an occasional pull-out of a SiC (or TiB_2) particle.

(5). Wear of the carbon graphite ring was greatest when in contact with reaction-sintered SiC, which caused nearly 5 times as much wear as did the other hard ring materials, probably due to abrasion of the carbon graphite face by pulled-out SiC grains.

From the work it can be concluded that ceramic and ceramic-coated seal ring materials both display very low wear. The friction and wear behavior of hard coatings can be as good as, if not better than (when one considers carbon graphite wear), that displayed by reaction-sintered silicon carbide. Because of their ductile metallic substrates, the coated rings are less prone to handling damage or gross fracture than monolithic silicon carbide and are easier to form in typical seal ring configurations. Therefore, despite potential problems with the spalling or wearing through of thin coatings and unresolved questions about corrosion resistance, further development of ceramic-coated seal ring materials is warranted.

3.0 ANALYTICAL STUDY

3.1 Introduction to Analytical Study

Contact spots are subjected to two types of loadings: mechanical loads consisting of shear and normal tractions at the contact interface, and thermal loading resulting from temperature gradients due to frictional heating. It is generally agreed that the interaction velocities during sliding are low enough to permit the use of uncoupled thermal stress theory in analyzing the phenomena [11]. Thus, two solutions are required: the temperature distribution around a frictionally-heated contact spot and the stress distribution due to the combination of surface tractions and temperature gradients. The problems have been treated previously using integral transform techniques for both two- and three-dimensional contacts on the surface of an elastic half-space [12,13]. Those techniques have recently been extended to the case of a layered elastic medium subjected to a moving contact [14]. Although those studies have given much insight into conditions around sliding contacts, they required several assumptions which limit their applicability for real sliding components: a single large body (half-space) was analyzed, all frictional heat was assumed to enter that body, and the body was elastic. The finite element method need not be subjected to those restrictions and that method has been used in the work reported here. Techniques have been developed for analyzing temperatures and stresses in two contacting solids in relative motion and they were used successfully in an earlier finite element thermal and thermoelastic analysis of sliding rings [5]. The methods enable both contacting bodies to be studied simultaneously, thus eliminating the need for assumptions about partioning of frictional heat or distribution of surface tractions. The earlier study [5] gave considerable insight into the reasons for thermocracking of sliding metallic ring surfaces. Based on that elastic analysis it was hypothesized, but not proven, that residual plastic strains could be responsible for propagation of thermally- induced cracks. Finite element methods can easily be used to predict residual stresses, as was shown in a recent elasto-plastic analysis of a body beneath a moving heat source [15].

3.2 ANALYTICAL TECHNIQUES

3.2.1 Contact Model.

Experiments similar to those reported above have shown that contact between two flat conforming rings is concentrated in several (1 to 5) patches, with a few small solid/solid contact spots ocurring within each patch [2]. For the case of a carbon graphite ring sliding against a metallic ring, the patches were found to remain approximately stationary with respect to the metallic ring surface, and similar results were found for carbon graphite rings sliding against ceramic or ceramic-coated rings in the experimental study reported in section 2 of this report. The contact spot sizes and locations determined in that experimental study were used here in setting the geometry of the contact model.

Based on the experimental evidence, it was assumed that each contact spot was identical and that the contacts were equally spaced aroung the ring circumference. A ring could therefore be divided into as many sections as the number of contact spots and only one such section would have to be analyzed. If, for example, there were three contact spots located at 120° intervals, the section to be studied would include one-third of each ring and would have a small region of solid-solid contact between the two rings in the center of the section.

Experimental work had shown that the contact spots were approximately rectangular in shape [2], extending further in the circumferential direction than radially. All tractions at the contact interface act in either circumferential (θ) or axial (z) directions, and in earlier analytical modelling [5,13] it was found that the most important temperature variations were those occurring in the θ-z plane. For this reason it was decided to analyze the problem only in the θ-z plane and to do a two-dimensional analysis. A typical two-dimensional ring section is shown in Figure 8 and a finite element mesh for the central section of the ring section is shown in Figure 9. It can be noted that a very fine grid is used in the contact region in the center of the mesh owing to the large temperature gradients there. No contact between top and bottom rings was allowed except within the central contact region.

Because contact did not occur over the entire radial thickness of the ring interface, some of the frictional heat generated in the contact zone was conducted in the radial direction into the contacting rings. Thus the thermal problem is not truly a two-dimensional one. To account for this out-of-plane

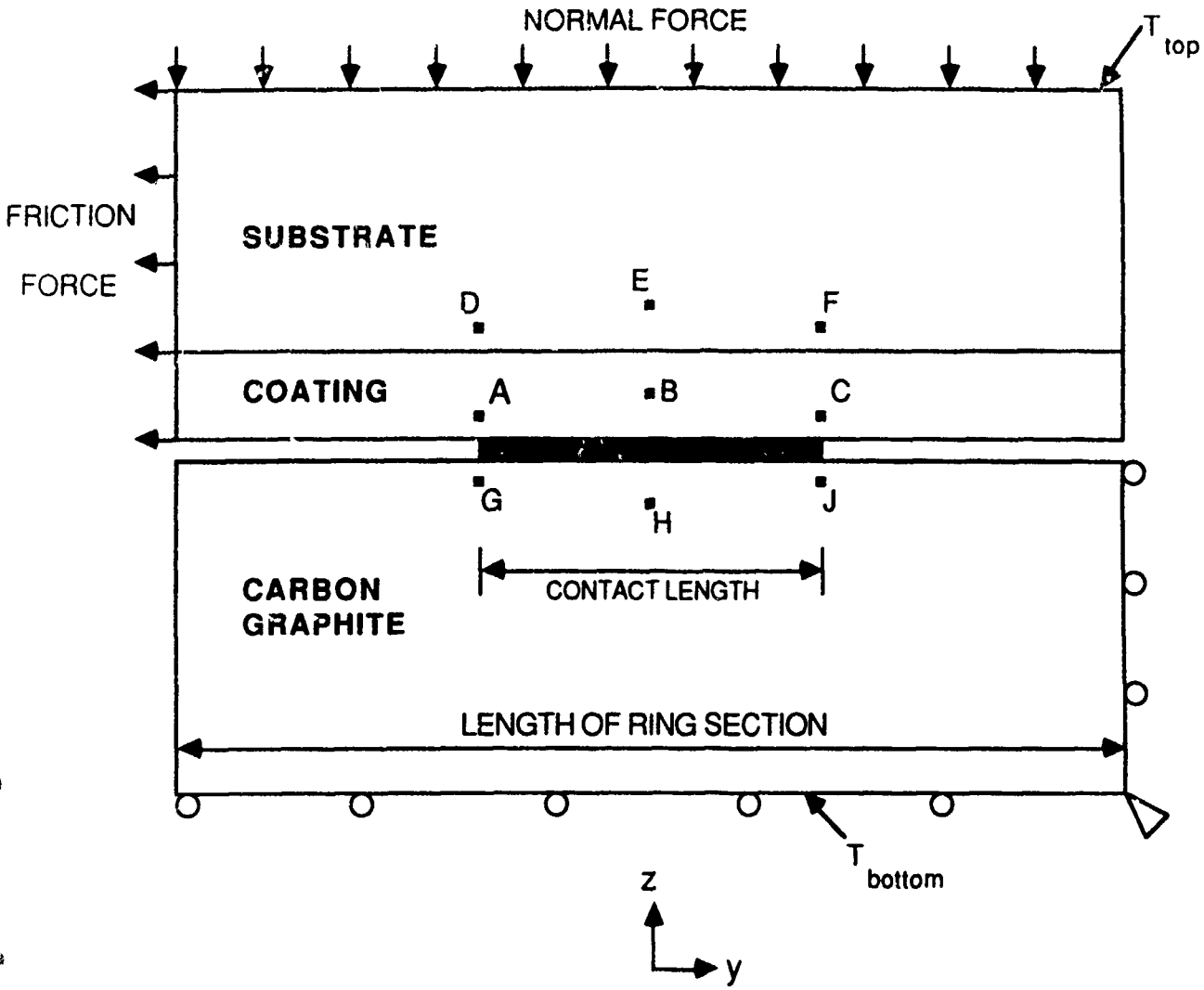

Figure 8 Schematic diagram of ring section showing boundary conditions for thermal and mechanical analysis and location of nine reference points.

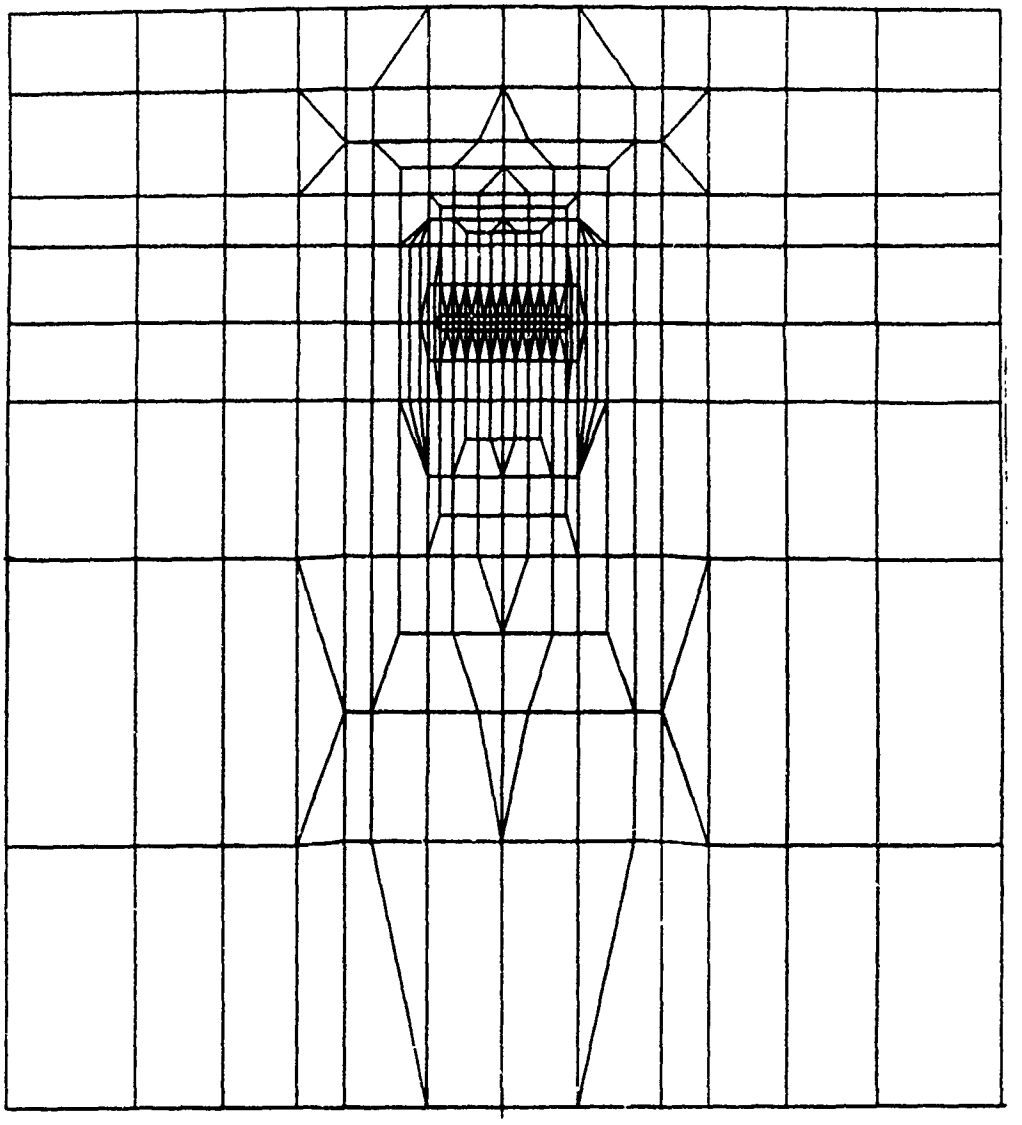

Figure 9 Central section of mesh generated by AUTOMESH for 1.0 mm long contact patch.

conduction a pseudo-three-dimensional thermal analysis was done by varying the thickness of two-dimensional finite elements. The flow of frictional heat from the contact zone produces streamlines that emanate from the contact. It was assumed that an arc normal to the streamlines in the r-z plane at a given (small) distance from the contact zone was an isotherm. The length of that arc could be considered to be the effective thickness of an element in the θ-z plane, an element with no temperature change in the radial direction. As heat flowed away from the contact the streamlines would spread, resulting in greater arc lengths and greater effective element thicknesses (and volumes). Thus, elements adjacent to the contact zone would have an effective thickness approximately equal to the radial extent of the contact, while elements further away would be progressively thicker, with the maximum thickness being the ring thickness. This idea is demonstrated in Figure 10, which shows the lower half of the model of Figure 8. A similar thickness distribution was used for the top half of the model. Following this idea, the thickness of each element in the mesh of Figure 9 was calculated and used in the thermal analysis.

Since each of the ring sections analyzed in this work was similar in shape to that shown in Figure 8, an automatic mesh generation routine (AUTOMESH) could be employed to create a mesh for any given section. In general the automatic mesh generation consisted of shrinking or stretching a well-proven prototype mesh such as that in Figure 9, subject to some constraints on element aspect ratio. The only input variables required by the mesh generation program were the section length, ring heights, ring thicknesses (radial), contact dimensions (radial and circumferential) and coating thickness.

3.2.2 Thermal Analysis.

The thermal analysis used a finite element program (THERMAP) developed specifically for studying the temperature distribution around sliding contacts [17,18]. The program differs from typical heat conduction codes in that it solves Fourier's Law for heat conduction in a solid moving relative to a coordinate system fixed in the contact zone, where frictional heat is being generated.

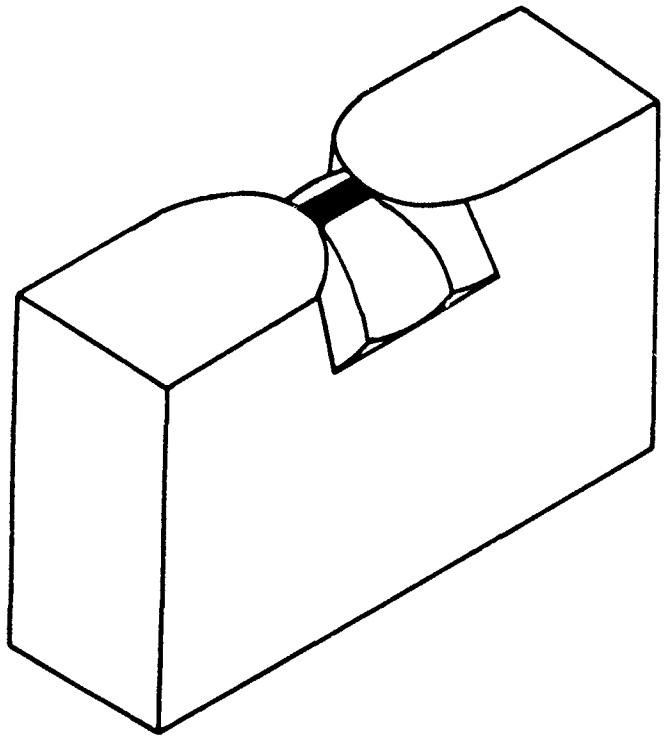

Figure 10 Three-dimensional view of lower ring section showing thickness variation around contact patch used in thermal analysis.

That equation may be written:

$$\nabla \cdot K\nabla T + Q - \rho C(\partial T/\partial t) - V \cdot \nabla T = 0 \qquad (1)$$

where K, ρ and C are the conductivity, density, and specific heat of the body, Q is the volumetric heat generation, T is temperature, t is time, and V is the sliding velocity. It has been shown that the temperature distribution around a sliding contact reaches a quasi-steady state, relative to the coordinate system fixed in the contact, very quickly, perhaps after sliding a distance equal to twice the contact length [11,18], so $\partial T/\partial t$ can be set equal to zero in most cases and a quasi-steady analysis can be done. The last term in equation (1), however, is present whenever one body is moving relative to the other and that convective-diffusion term has been found to cause numerical oscillations at high sliding velocities (or high Peclet numbers) [18]. After investigating a number of ways to avoid the difficulty, the streamline upwind technique [19] was implemented because it was found to produce a substantial improvement in solution at high Peclet numbers without excessive computing effort [18].

The boundary conditions for the thermal solution included prescribed temperatures on the top and bottom surfaces of the model in Figure 8. Those temperatures were set equal to temperatures measured at those locations in the experimental program. Convection to ambient air was assumed at the free surface of the rotating ring and reasonable convection coefficients were chosen from the heat transfer literature. A heat flux equal to the product of contact pressure times friction coefficient times velocity was input to the interface between the two rings within the contact zone. It was earlier found that the form of the contact pressure distribution had little effect on the temperature distribution [2], so a uniform heat flux distribution was assumed. The ring section being analyzed was assumed to be identical to the ones on either side of it, and to insure this the nodal temperatures on the right hand edge of the model in Figure 8 were set equal to those on the left hand edge.

3.2.3 Stress Analysis.

Analysis of the stresses and deformations around the sliding contact was done using the ADINA finite element program. The boundary conditions for the analysis are shown in Figure 8. The friction and normal forces were those measured or applied in the experimental phase of the work. Since only one section of the ring was analyzed and it was assumed that the ring was composed of n identical

sections, the friction and normal forces applied to the model were 1/n times the measured force values. The two contacting rings were analyzed together and no attempt was made to insure a uniform distribution of contact pressure or shear traction within the predetermined contact zone. Techniques were developed earlier for determining the contact pressure distribution after a thermomechanical analysis of a sliding contact [2]. Those techniques were used here to determine the contact pressure distribution and to insure that compressive normal tractions actually existed everywhere within the assumed contact zone. Methods are also available for insuring that the friction traction is everywhere equal to the normal pressure times the friction coefficient [20]. Those techniques were not used here because it was believed, based on earlier analyses [2,5], that the stress field near a sliding contact is dominated by the thermal contribution, which is not significantly affected by distribution of surface tractions. Instead a tangential force equal to the measured value was applied as shown in Figure 8.

In order to determine the relative contributions of the mechanical and thermal loads, the loads were applied in separate increments. In the first increment the mechanical loads were applied with the body at uniform temperature. The temperatures were then added as ramp functions over the next increment. During the fourth increment the temperatures were returned to their uniform value, while the mechanical loads were removed in the fifth increment.

3.2.4 Analysis Procedure.

A suite of interconnected programs was created to enable the analysis to proceed automatically once the problem geometry and boundary conditions were defined. Those data could be input either to a data file, for batch mode operation, or interactively. The flow chart shown in Figure 11 shows the various programs called automatically during the analysis, which was carried out on a Vax 11-785. In addition to the automatic mesh generation program, AUTOMESH, the thermal analysis program, THERMAP, and the stress analysis program, ADINA, there were several other programs interlaced in the analysis for pre- or post- processing of data. The output was primarily in the form of plots of calculated temperature and stress distributions, along with printed information about the maximum stress and temperature values within each of the materials: moving ring, stationary ring substrate, and ceramic coating on stationary ring.

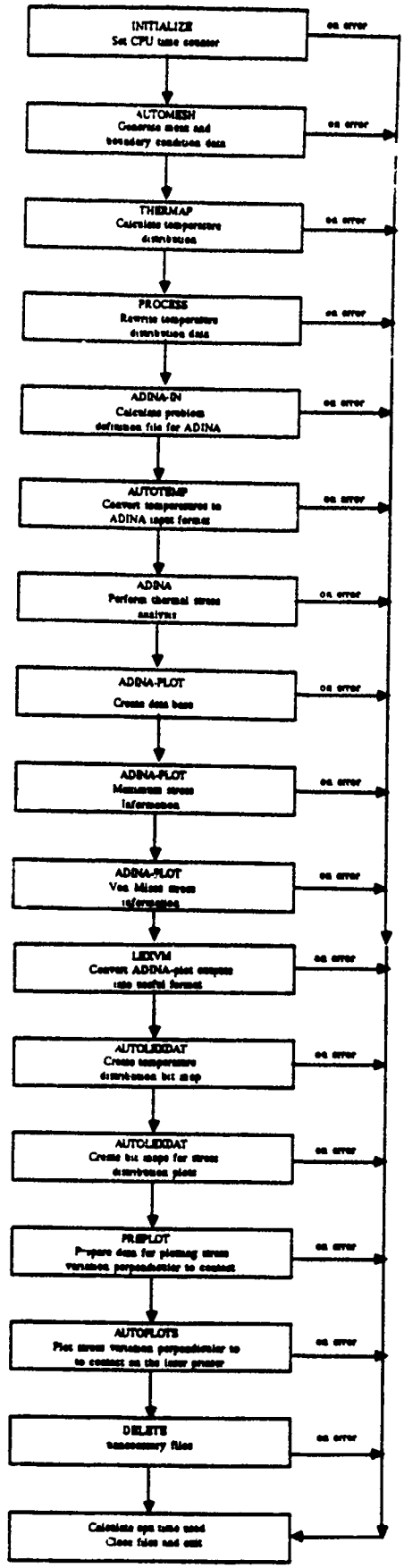

Figure 11 Flow chart for automated analysis.

3.3 ANALYTICAL RESULTS AND DISCUSSION

3.3.1 Thermoelastic Analysis of Baseline System

The system chosen to serve as the baseline model for this analysis was composed of a mild steel ring with a tungsten carbide coating in sliding contact with a ring made of carbon graphite. This system has been the focus of the experimental phase of this study, and the conditions studied here were based on measurements made in that test program. The axial thickness of the coated steel ring was 6.43 mm, while that of the carbon graphite ring was 10 mm. The plasma-sprayed tungsten carbide coating on the contacting surface of the steel disk was approximately 0.2 mm thick. The 50 mm diameter rings were in solid/solid contact at two identical contact patches located 180° from one another. Thus a single ring section of circumferential length 79 mm could be analyzed. A typical contact patch was assumed to be 1 mm wide in the circumferential direction and 1 mm deep in the radial direction. The normal force on a contact was assumed to be 100 N, with a coefficient of friction of 0.1. Steady-state temperatures of the top (non-contacting) face of the metallic ring and the bottom face of the carbon graphite ring were both assumed to be 150°C. The metallic ring was rotating at 1800 rpm relative to the stationary carbon ring, but the contact patch was stationary with respect to the metallic ring. Thus, the carbon ring was assumed to be moving at a velocity of 4.71 m/s in the positive z direction relative to the contact, while the metallic ring had zero velocity relative to the contact region.

A quasi-steady state thermal analysis of the baseline system produced the temperature distribution shown in Figure 12a. It can be seen that the highest temperature occurred on the contact interface. The maximum temperature was 285°C in this case, giving a temperature rise of 135°C above the back face temperatures. The temperature distribution in the metallic ring was relatively symmetrical about the contact center, while that in the carbon ring was skewed toward the direction of motion. This is a typical form of temperature distribution around a sliding contact [17]. A close-up of the temperature isotherms in the contact region is shown in Figure 12b. The contact extended from -0.5 to +0.5 mm, and the peak temperature occurred a bit to the right of the center of contact. Only a slight distortion of the isotherms can be noted as they pass from the tungsten carbide coating into the mild steel substrate.

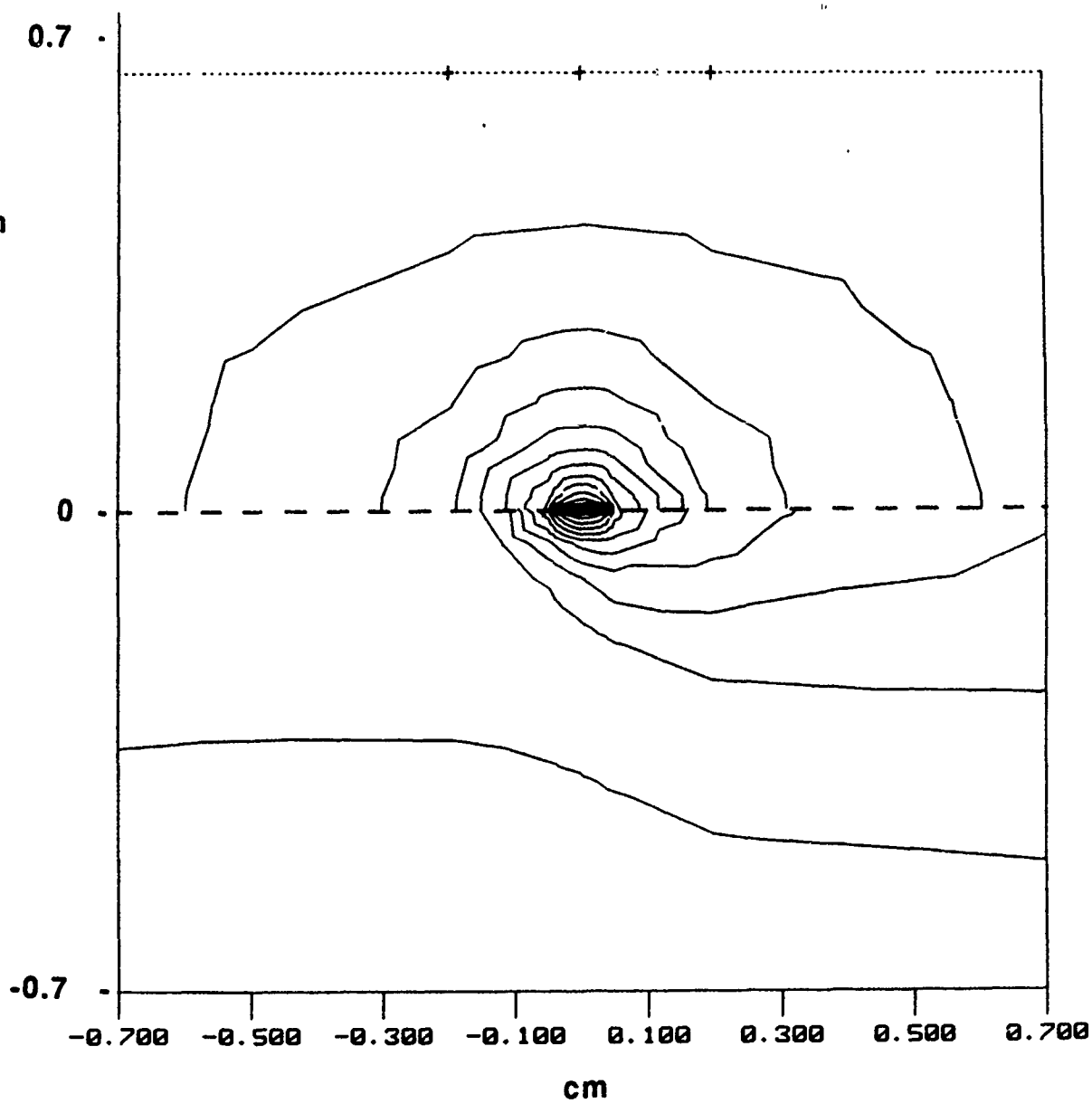

Figure 12a Isotherms in ring section for baseline case. Carbon graphite ring is on bottom. Ceramic coating is 0.02 cm thick. Circumferential (y) direction is horizontal in Figure; axial (z) is vertical.

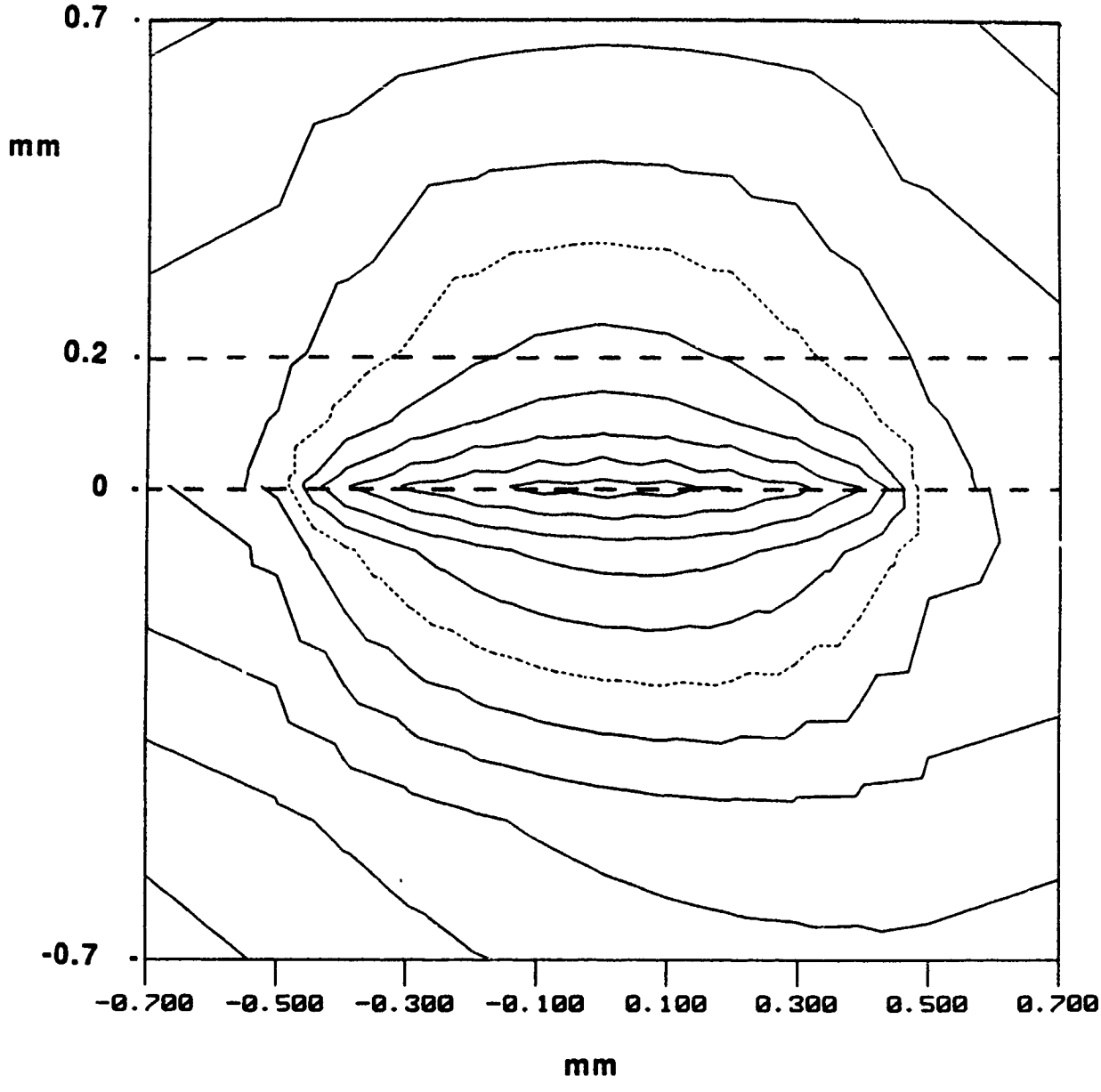

Figure 12b Isotherms in contact region of ring section for baseline case.
Contact patch extends from y = -0.5 mm to y = 0.5 mm.
Ceramic coating is 0.2 mm thick.

The thermal conductivity of the tungsten carbide material is 100 W/mK, approximately twice that of mild steel (51.9 W/mK).

The stress analysis was carried out incrementally, with the mechanical tractions first being applied and then the temperatures being added. This allowed a study of the relative contributions of mechanical and thermal loadings. Results are shown in Table 2 for nine points in the contact region, three each in coating, substrate and carbon. The location of the nine points is shown in Figure 8. A plane strain situation was assumed in this case, as in all other cases.

It can be seen in Table 2 that the mechanical loading produced a stress state that was predominantly compressive. The normal contact pressure (σ_{zz}) was non-uniform, ranging from nearly zero at the right edge of the contact to between 100 and 200 MPa at the left edge. This is due to the effective moment exerted about the center of contact by the applied friction force (Figure 8). The circumferential (y-direction) stress was compressive except for a small tensile stress in the coating at the righthand edge of the contact. That tensile stress would be too small to cause coating fracture. This is in agreement with a recent analysis of a layered sliding contact by Ju [14].

The addition of temperature gradients to the mechanical loads caused very little change in the distribution of axial stress σ_{zz} or shear stress τ_{yz}, but resulted in substantial changes in out-of-plane normal stress σ_{xx} and in the circumferential stress σ_{yy}. The radial stress σ_{xx} is caused by the plane strain nature of the localized thermal deformation, and its relatively large magnitude could contribute to plastic deformation in coating or substrate. The most significant result of the stress analysis, however, is the very substantial tensile stress σ_{yy} which occurred in the coating, especially near the righthand edge of the contact (Point C). The temperature gradients near the contact produced a change in σ_{yy} that was tensile in the coating and compressive in the much thicker substrate. The tensile thermal contribution to the circumferential stress in the coating was large enough to outweigh the predominantly compressive contribution from the mechanical loads, especially near the trailing edge of the contact. The resulting tensile stress could be responsible for the radial cracks, called thermocracks, noted in some ceramic coatings on seal ring surfaces [16]. The tensile stresses calculated here are less than the tensile strength of tungsten carbide, and that may be a reason no cracks were noted in tests of WC-coated rings described earlier. As is shown below, however, with other coated systems the

TABLE 2

CONTRIBUTION OF MECHANICAL AND THERMAL LOADINGS TO STRESS AT VARIOUS POINTS IN TUNGSTEN CARBIDE COATING, MILD STEEL SUBSTRATE AND CARBON GRAPHITE MATING RING
- THERMOELASTIC ANALYSIS -

	STRESS IN MPa							
	MECHANICAL LOADS ONLY				MECH. LOADS + TEMPERATURES			
	σ_{xx}	σ_{yy}	σ_{zz}	τ_{yz}	σ_{xx}	σ_{yy}	σ_{zz}	τ_{yz}
COATING								
A	- 239	- 579	- 275	- 135	- 575	+ 198	- 285	- 146
B	- 63	- 175	- 51	- 10	- 480	+ 676	- 42	- 20
C	+ 6	+ 1	+ 20	- 23	- 326	+ 796	+ 16	- 16
SUBSTRATE								
D	- 28	- 29	- 68	0	- 518	- 181	- 97	- 6
E	- 24	- 37	- 45	- 21	- 511	- 171	- 26	- 20
F	- 18	- 44	- 21	- 21	- 512	- 198	- 52	- 15
CARBON GRAPHITE								
G	- 54	- 61	- 120	+ 38	- 62	- 29	- 96	+ 12
H	- 24	- 28	- 51	+ 22	- 37	+ 1	- 44	+ 22
J	- 3	- 4	- 6	+ 13	- 11	+ 28	+ 17	+ 38

NOTE: The following parameters were used in the analysis: coating thickness = 0.2 mm, contact length = 1.0 mm, normal load = 100 N, friction coefficient = 0.1, sliding velocity = 4.71 m/s. The point locations are shown in Figure 8.

circumferential tensile stresses could exceed the tensile strength of the coating, resulting in surface-originated radial cracks.

The results shown in Table 2 assumed purely elastic deformation. The effective (von Mises) stress determined in that analysis was rather large in both coating and substrate, however, so some plastic deformation could be anticipated. Figure 13 shows the isobars (lines of constant effective stress) for the baseline thermoelastic case. It can be seen that much of the coating in the contact zone had a high effective stress, with the peak effective stress in both coating and substrate occurring near the point of maximum contact temperature. Thermal effects were found to be the major contributor to those high effective stresses and therefore would be the dominant factor leading to yielding in either coating or substrate.

3.3.2 Thermoplastic Analysis of Baseline System

In order to study the effects of plastic deformation on the stress state around the contact, several thermo-plastic analyses of the baseline system were done using the same suite of programs described above. The materials were assumed to have a temperature-dependent yield strength and isotropic hardening post-yield behavior. In one case the substrate material was assumed to have a room temperature yield strength of 345 MPa, about 20% less than the maximum effective stress calculated in the thermoelastic case, while the yield strength of the coating material was kept at 1300 MPa, high enough to keep that material within the elastic range. In another case the coating material was assumed to have a yield strength of 900 MPa, soft enough for yielding to occur, while the substrate was assumed to have a 500 MPa yield strength, thus keeping it elastic. Results of those studies are presented in Table 3. It can be seen that yielding of either substrate or coating resulted in a lower effective stress in both materials and a lower maximum tensile stress in the coating. Thus, either a softer coating or a softer substrate would lessen the chances of coating fracture during a single contact encounter. After the contact spot moved elsewhere, however, there would be residual stress at the contact location. As can be seen in Table 3 the residual stress in the coating would be tensile, but it would not be large enough to cause coating failure by itself. If further contact occurred at the same

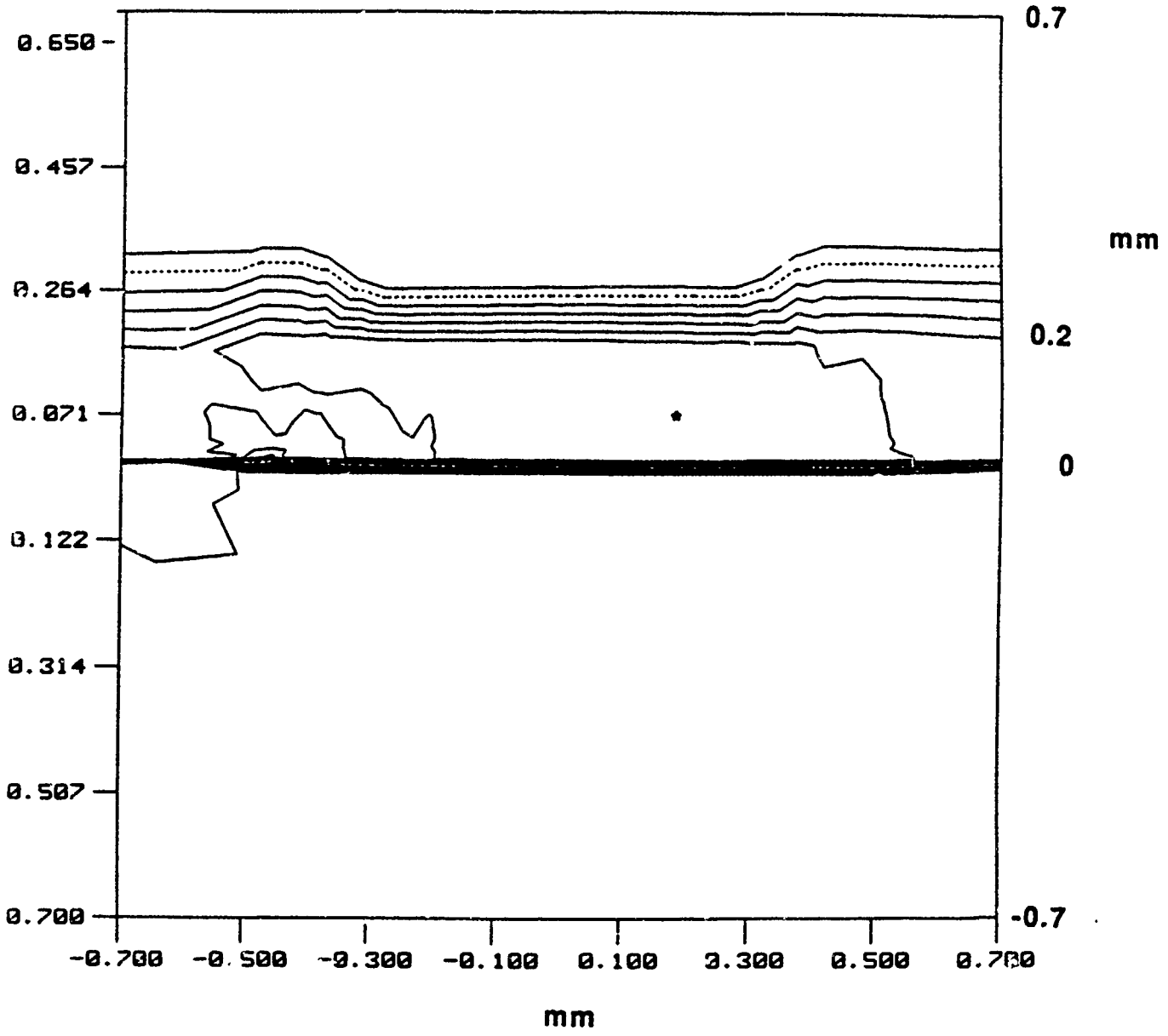

Figure 13 Lines of constant effective stress (isobars) in contact region of ring section for baseline case. Contact patch extends from y = -0.5 mm to y = 0.5 mm. Ceramic coating is 0.2 mm thick.

TABLE 3

INFLUENCE OF PLASTIC DEFORMATION ON MAXIMUM TENSILE STRESS IN COATING AND MAXIMUM EFFECTIVE STRESSES IN COATING AND SUBSTRATE

	MAXIMUM TENSILE STRESS IN COATING	MAXIMUM EFFECTIVE STRESS	
		COATING	SUBSTRATE
THERMOELASTIC ANALYSIS	797	1034	437
THERMOPLASTIC ANALYSIS - YIELDING ONLY IN COATING	714	900	423
TYPICAL RESIDUAL STRESS	10	100	10
THERMOPLASTIC ANALYSIS - YIELDING ONLY IN SUBSTRATE	764	1022	346
TYPICAL RESIDUAL STRESS	20	20	100

NOTE: The yield strengths of coating and substrate were set at 900 MPa and 345 MPa, respectively. All stresses are in units of MPa.

location, though, the residual tensile stress would augment the tensile stress from thermal and mechanical loading, increasing the likelihood of coating fracture in subsequent contact occurrences. Thus, in addition to the thermoelastic tensile stresses discussed above, low-cycle fatigue could contribute to thermocracking of coated systems. A related low-cycle fatigue mechanism was proposed by Fec and Sehitoglu [21] to account for thermocracking of railroad wheels.

3.3.3 Effect of Material, Geometric, and Operating Parameters on Stress Distribution

An extensive series of analyses was carried out to study the influence of material properties, coating and contact dimensions, normal and friction forces, and velocity on the stresses that could lead to coating failure. Since the baseline analysis showed that the stress in coating and substrate were greatest for the thermoelastic case, and since harder materials seem to be the most likely candidates for future contact applications, elastic behavior was assumed for most of the analyses. Results are presented in Tables 4 to 7.

In each of the cases in Table 4 a single material parameter was changed from its baseline value. The properties of most interest were the modulus of elasticity E, coefficient of thermal expansion α, and thermal conductivity K of the substrate and coating materials. Since thermal conductivities of each material affect the temperatures that are the driving force responsible for the high stresses, it is not surprising that an increase in thermal conductivity of either coating or substrate led to lower stresses in each of the components. The conductivity of the coating was found to have much less effect on stress than that of the substrate, presumably because the high temperature in the more massive substrate and the resulting thermal expansion were responsible for the tensile stress within the thin coating. A substantial decrease in coating stress could be brought about by choosing a more conductive substrate which could transfer more of the frictional heat away from the contact region.

The effects of modulus of elasticity and coefficient of thermal expansion were quite large and can be explained by thermal deformation considerations. An increase in the elastic modulus of one of the two materials raised the stress in that material but had a much smaller influence on stress within the other material. This was to be expected for a laminated composite material subjected to thermal deformation. In the baseline analysis it was learned that the difference in thermal expansion between

TABLE 4

EFFECT OF MATERIAL PROPERTIES ON MAXIMUM TEMPERATURES AND STRESSES
- THERMOELASTIC ANALYSIS -

PROPERTY CHANGED FROM BASELINE VALUE	CHANGE IN CALCULATED VALUES (FROM BASELINE) MAXIMUM TEMPERATURE	MAX. EFFECTIVE STRESS CARBON	SUBSTRATE	COATING
$E_{coating}$ up by 100%		- 8.1%	+ 0.9%	+ 76.5%
$E_{coating}$ down by 50%		+ 7.0%	- 0.2%	- 44.4%
$\alpha_{coating}$ up by 100%		+ 8.1%	+ 0.2%	+ 35.8%
$\alpha_{coating}$ down by 50%		- 4.1%	+ 0.8%	+ 4.2%
$K_{coating}$ up by 100%	- 23.7%	- 3.5%	- 3.5%	- 4.0%
$K_{coating}$ down by 50%	+ 34.8%	+ 3.5%	+ 1.8%	+ 4.0%
$E_{substrate}$ up by 100%		+ 2.3%	+ 72.0%	+ 2.1%
$E_{substrate}$ down by 50%		- 11.6%	- 55.8%	- 17.5%
$\alpha_{substrate}$ up by 100%		+ 54.7%	+ 73.3%	+ 79.5%
$\alpha_{substrate}$ down by 50%		- 30.2%	- 55.6%	- 36.2%
$K_{substrate}$ up by 100%	- 29.6%	- 14.0%	- 17.0%	- 17.2%
$K_{substrate}$ down by 50%	+ 45.9%	+ 24.4%	+ 26.7%	+ 27.9%

NOTE: Baseline system had the following properties at room temperature: $E_{coating}$ = 614 GPa, $\alpha_{coating}$ = 4 E-6/°C, $K_{coating}$ = 100 W/mK, $E_{substrate}$ = 192 GPa , $\alpha_{substrate}$ = 10.5 E-6/°C , $K_{substrate}$ = 51.9 W/mK . All systems had the same geometric configuration, loads, and velocity.

TABLE 5

EFFECT OF LOADS AND VELOCITY ON MAXIMUM TEMPERATURES AND STRESSES
- THERMOELASTIC ANALYSIS -

NORMAL LOAD FRICTION COEFF. AND VELOCITY	MAXIMUM TEMPERATURE RISE	MAXIMUM EFFECTIVE STRESS (MPa)		
		CARBON	SUBSTRATE	COATING
BASELINE	135°C	130	437	1034
NORMAL LOAD =200 N	270°C	245	597	1440
NORMAL LOAD = 50 N	67.5°C	73	356	855
FRICTION COEFF. = 0.2	270°C	195	616	1541
FRICTION COEFF. = 0.05	67.5°C	97	347	830
VELOCITY = 9.42 m/s	268°C	145	603	1505
VELOCITY = 2.355 m/s	68°C	123	352	850

NOTE: Unless otherwise noted, the load, friction, and sliding velocity were those of the baseline system: NORMAL LOAD = 100 N, FRICTION COEFFICIENT = 0.1, VELOCITY = 4.71 m/s. All systems had the same material properties as the baseline system in Table 4.

TABLE 6

EFFECT OF CONTACT GEOMETRY AND COATING THICKNESS
ON MAXIMUM SURFACE TEMPERATURE AND EFFECTIVE STRESSES
- THERMOELASTIC ANALYSIS -

COATING THICK. mm	CONTACT LENGTH mm	CONTACT DEPTH mm	MAXIMUM TEMPERATURE RISE	MAX. EFFECTIVE STRESS (MPa) CARBON	SUBSTRATE	COATING
0.1	1.0	1.0	140°C	136	461	1188
0.2	1.0	1.0	135°C	130	437	1034
0.4	1.0	1.0	126°C	112	409	840
1.0	1.0	1.0	125°C	106	365	654
0.2	0.5	1.0	167°C	209	133	900
0.2	2.0	1.0	106°C	108	424	957
0.2	1.0	0.5	154°C	130	439	1042
0.2	1.0	2.0	120°C	128	432	1022

NOTE: All systems had the same material properties and the same assumed normal load, friction coefficient, and velocity (the baseline values in Tables 4 and 5).

TABLE 7

EFFECT OF VARIOUS PARAMETERS ON MAXIMUM TENSILE STRESS IN COATING
- THERMOELASTIC ANALYSIS -

VARIABLE CHANGED FROM BASELINE VALUE	LARGEST TENSILE PRINCIPAL STRESS IN COATING (MPa)
BASELINE	797
COATING THICKNESS REDUCED BY 50%	982
CONTACT LENGTH DECREASED BY 50%	1270
FRICTION COEFFICIENT INCREASED BY 100%	1346
FRICTION COEFFICIENT DECREASED BY 50%	266
$\alpha_{coating}$ DECREASED BY 50%	1079
$\alpha_{coating}$ INCREASED BY 100%	233

NOTE: Unless otherwise noted, the load, friction, and sliding velocity were those of the baseline system: normal load = 100 N, friction coefficient = 0.1, velocity = 4.71 m/s. The baseline coating thickness, the contact length and contact depth were 0.2 mm, 1.0 mm, and 1.0 mm, respectively, and the baseline material properties were those given in Table 4.

substrate and coating was primarily responsible for tensile stress within the coating (and compressive stress in the substrate). Thus, it is not surprising that an increase in the substrate material's thermal expansion coefficient caused a large increase in stress in both materials. The fact that an increase in the coating material's expansion coefficient also caused an increase in coating stress appears perplexing, until one realizes that thermal expansion of the coating caused an increase in the out-of-plane compressive stress σ_{xx} , and this led to an increase in the effective (or von Mises) stress. In fact, the potentially damaging tensile stress σ_{yy} in the coating was reduced by an increase in thermal expansion of the coating, as can be seen in Table 7.

The effects of normal and friction forces and velocity on stresses and temperatures around the contact are given in Table 5. It can be seen that an increase in either normal force or friction coefficient led to substantial increases in stress in all three materials. This is due not to the increased stress one normally associates with higher loads, but to increases in temperature and the corresponding thermal deformation. A doubling of either normal force or friction coefficient resulted in a doubling of the temperature increase due to frictional heating, and that in turn led to substantially increased thermal stress. Not only was the effective stress increased, but the tensile stress in the coating was drastically affected by the increased frictional heating, as can be seen from the friction results in Table 7. This may account for the fact that cracking of coated rings was observed by Tribe [16] in tests at very high normal load, but not in our recent tests at a much lower load. The effect of velocity is similar to that of friction, and results from higher surface temperatures owing to greater frictional heating. Although the heat generation rate is the same if either friction or velocity is doubled, the surface temperatures and corresponding thermal stresses are a bit lower for the increased velocity case because of the effective cooling by the convective-diffusion term in equation (1). The normal force has less of an effect on the maximum coating stresses than the friction or velocity because the mechanical stresses caused by the larger normal force tend to be opposite in sign to the thermal stresses, as was seen in Table 2.

The influence of coating thickness and contact patch size is presented in Table 6. An increase in the thickness of the hard coating resulted in a slightly higher contact temperature and a larger increase the stress in each material. As the coating became thinner, more of the substrate was exposed to higher temperature, resulting in more thermal deformation and greater coating stress. Along with the

increase in the effective stress of the coating there was a corresponding increase in the tensile stress, as can be seen in Table 7. Changes in the size of the contact patch also had a very significant effect on contact temperature and thermal deformation. A larger contact had a lower frictional heat flux, resulting in lower surface temperatures. As expected, this led to lower stresses, whether the larger contact was brought about by an increase in circumferential contact length or radial contact depth. It is somewhat surprising to note, however, that a smaller contact length brought about a smaller effective stress. The reason was similar to the one discussed above for the case of increased coating thermal expansion. The shorter contact had higher temperatures, but the higher temperatures were confined to a smaller region. Thus, the coating material was subjected to more thermal expansion near the center of the contact, and the substrate to less, resulting in lower effective stresses. There was still a very substantial tensile stress at the trailing edge of the shorter contact (point C in Figure 8), however, as can seen in Table 7.

3.4 CONCLUSIONS FROM ANALYTICAL STUDY

The finite element package used here to study temperatures and stresses around a sliding conforming contact gave much insight into the mechanisms of thermocracking of hard ceramic coatings and the factors that affect it. It was found that the stress field around a sliding contact is dominated by the thermal contribution resulting from frictional heating. That contribution tends to cause tensile stresses in the coating, acting in the sliding direction. These tensile stresses could be large enough to cause cracking of the coating. Although the tensile stresses would be reduced by plastic deformation in either coating or substrate, such plastic deformation would result in residual tensile stress in the coating. The residual stress could lead to a low-cycle fatigue crack initiation by augmenting the thermomechanical tensile stress in the coating. To avoid this a harder substrate material would be desirable.

It was found that the stress in the coating could be substantially reduced by operating at lower normal load or lower velocity, or by achieving a lower friction coefficient. A reduction in coating stress could also be achieved by having a thicker coating or a coating with a lower modulus of

elasticity or higher thermal conductivity. An increase in coating thermal expansion coefficient would result in significantly lower tensile stress in the coating but more likelihood of plastic deformation. The properties of the substrate proved to be at least as important as those of the coating, with decreased coefficient of thermal expansion (or less difference between $\alpha_{substrate}$ and $\alpha_{coating}$), decreased modulus of elasticity, and increased thermal conductivity of the substrate material leading to significant reductions in stress in both coating and substrate.

REFERENCES

1. Kennedy, F.E., and Grim, J.N., "Observation of Contact Conditions in Mechanical Face Seals", ASLE Trans., 27 (1984), 122-128.

2. Kennedy, F.E., Grim, J.N. and Chuah, C.K., "An Experimental/Theoretical Study of Contact Phenomena in Mechanical Face Seals", in Developments in Numerical and Experimental Methods Applied to Tribology, Butterworths, Lyon, 285-291, (1984).

3. Kennedy, F.E., Chuah, C.K. and Brote, F.O.W., "Thermomechanical Contact Phenomena in Face Seals", Wear, 102 (1985), 127-140.

4. Johnson, R.L. and Schoenherr, K., "Seal Wear", Wear Control Handbook, M.B. Peterson and W.O. Winer, eds., ASME, N.Y. 1980, 727-753.

5. Kennedy, F.E. and Karpe, S.A., "Thermocracking of a Mechanical Face Seal", Wear, 79, 21-36, (1982).

6. Lashway, R.W., Seshadri, S.G., and Srinivasan, M., "Various Forms of Silicon Carbide and Their Effects on Seal Performance," Lubrication Engineering, 40 (1984), 356-363.

7. Wu, C.C., Rice, R.W., Platt, B.A. and Carrle, S., "Wear and Microstructure of SiC Ceramics", Ceramic Eng'g. & Science Proc., 6 (1985), 1023-1039.

8. Tribe, F., "Seawater-Lubricated Mechanical Seals and Bearings: Associated Materials Problems", Lubrication Engineering, 39 (1983), 292-299.

9. Hinterman, H.E., "Adhesion, Friction and Wear of Thin Hard Coatings, Wear, 100 (1984), 381-397.

10. Derby, J., Seshadri, S.G., Srinivasan, M., "Non-Lubricated Sliding Wear of Al_2O_3, PSZ, and SiC", Proc. 4th Int'l Symp. on Fracture Mechanics of Ceramics, Blacksburg, VA. (1985).

11. Ling, F.F., Surface Mechanics, Wiley, New York, 1972.

12. Mow, V.C. and Cheng, H.S., "Thermal Stresses in an Elastic Half-Space Associated with an Arbitrarily Distributed Heat Source", Z. Agnew. Math. Phys., 18, 500-507, (1967).

13. Huang, J.H. and Ju., F.D., "Thermomechanical Cracking due to a Moving Friction Load", Wear, 102, 81-97 (1985).

14. Ju., F.D. and Chen, T.Y., "Thermomechanical Cracking in Layered Media from Moving Friction Load", ASME J. Tribology, 106, 513-518, (1984).

15. Mishra, A. and Prasad, T., "Residual Stresses due to a Moving Heat Source", Int. J. Mech. Sci., 27, 571-581, (1985).

16. Tribe, F.J. and Green, G.A., "Assessment of Mechanical Seal Face Materials Under Controlled Interface Torque", Lubrication Engineering, 42, 686-693, (1986).

17. Kennedy, F.E., "Surface Temperatures in Sliding Systems - A Finite Element Analysis", ASME J. Lubrication Technology, 103, 90-96, (1981).

18. Kennedy, F.E., Colin, F., Floquet, A. and Glovsky, R., "Improved Techniques for Finite Element Analysis of Sliding Surface Temperatures", in Developments in Numerical and Experimental Methods Applied to Tribology, Butterworths, Lyon, 138-150, (1984).

19. Brooks, A.N. and Hughes, T.J.R., "Streamline Upwind/Petrov Galerkin formulations for Convective Dominated Flows", Computer Meth. in Appl. Mech. & Engg., 32, 199-259, (1982).

20. Bathe, K.-J. and Chaudhary, A., "On Finite Element Analysis of Large Deformation Frictional Contact Problems", in Unification of Finite Element Methods, H. Kardestuncer, Ed., Elsevier Science Publishers, 123-147, (1984).

21. Fec, M.C. and Sehitoglu, H., "Thermal-Mechanical Damage in Railroad Wheels due to Hot Spotting", Wear, 102, 31-42, (1985).